Journal Pre-proofs

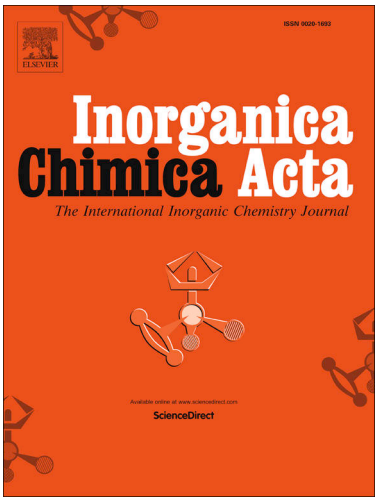

Chinese-Lantern shaped [$Mn^{II}_{2}Mn^{III}_{6}Na^{I}_{3}$] cluster assembled from Schiff base and azide bridges: Synthesis, magnetic study and catecholase-like activity

Krishna Chattopadhyay, Biswarup Dutta, Shyamali Dutta, Anupama Manna, Gavin A. Craig, Manas Mandal, Mark Murrie, Debashis Ray

PII: S0020-1693(24)00361-X
DOI: https://doi.org/10.1016/j.ica.2024.122270
Reference: ICA 122270

To appear in: *Inorganica Chimica Acta*

Received Date: 29 March 2024
Revised Date: 19 June 2024
Accepted Date: 19 July 2024

Please cite this article as: K. Chattopadhyay, B. Dutta, S. Dutta, A. Manna, G.A. Craig, M. Mandal, M. Murrie, D. Ray, Chinese-Lantern shaped [$Mn^{II}_{2}Mn^{III}_{6}Na^{I}_{3}$] cluster assembled from Schiff base and azide bridges: Synthesis, magnetic study and catecholase-like activity, *Inorganica Chimica Acta* (2024), doi: https://doi.org/10.1016/j.ica.2024.122270

Chinese-Lantern Shaped [$Mn^{II}_2Mn^{III}_6Na^{I}_3$] Cluster Assembled from Schiff Base and Azide Bridges: Synthesis, Magnetic Study and Catecholase-like Activity

Krishna Chattopadhyay,[a,b] Biswarup Dutta,[a] Shyamali Dutta,[a] Anupama Manna,[a] Gavin A. Craig,[c] Manas Mandal,[d] Mark Murrie,[c] Debashis Ray[a*]

[a]*Department of Chemistry, Indian Institute of Technology, Kharagpur 721302, India*

[b]*Department of Chemistry, Calcutta University, Kolkata 700 009, India*

[c]*School of Chemistry, University of Glasgow, Glasgow G12 8QQ, United Kingdom*

[d]*Department of Chemistry, Sree Chaitanya College, Habra, WB 743268, India*

Abstract

A multisite Schiff base, H_2damp, derived from the condensation of *o*-vanillin and a sterically constrained amino-alcohol (2-amino-2-methylpropan-1-ol) was utilized to isolate a new mixed valence heterometallic complex [$Na_3Mn^{III}_6Mn^{II}_2$(damp)$_6$(μ_4-O)$_2$($\mu_{1,3}$-O_2CCH_3)$_2$($\mu_{1,1}$-N_3)$_6$($\mu_{1,1,3}$-N_3)(H_2O)$_2$]·5H_2O·CH_3OH (**1**). Room temperature reaction of H_2damp in MeOH with Mn(II) acetate and NaN_3 provided the complex having $Mn^{II}_2Mn^{III}_6Na^{I}_3$ core. X-ray structure determination revealed the use of azide ancillary ligands for the growth of the complex on ligand-bound Mn^{III}_3O fragments. The variable temperature magnetic characterization of **1** revealed intramolecular anti-ferromagnetic exchange interactions. Complex **1** also showed catalytic property for the aerial oxidation of 3,5-di-*tert*-butyl catechol (3,5-$DTBCH_2$) with a turnover number (k_{cat}) of 392 h^{-1}. EPR and mass spectrometric analysis established the probable mechanism of catalytic oxidase reactivity on the model substrate. In EPR study the characteristic peak at $g \sim 2$ allowed us to spot the presence of an organic radical confirming the conversion of $DTBCH_2$ to DTBQ in radical pathway.

Introduction

Synthetic coordination chemistry has seen huge advancement in recent years through utilization of simple Schiff bases for aggregation of multiple number of manganese ions under direct coordination control of several ligand anions. [1-3] Such complexes, as representative analogues, have drawn much attention because of their similarity to multimetallic cofactors [4] and in the oxygen-evolving center (OEC) of photosystem II. [5-8] Studies on such model analogues can offer a rational understanding for the stepwise growth of the trinuclear to octanuclear manganese complexes.

Such synthetic endeavor can be targeted to the development of literature unknown family of single-molecule magnets (SMMs), which can function as nanoscale magnetic particles below their characteristic blocking temperature, T_B.[9] Thus choice of new ligand system and reaction methodology would be worth exploring for the production of new family of SMMs. Such multimetallic aggregates of manganese ions show a variety of shapes and topologies like triangles,[10] cubes,[11] and butterflies,[12] to wheels,[13] discs,[14] rods,[15] truncated cubes,[16] super-cubanes,[17] and super-tetrahedrons.[18] Majority of them are obtained via self-assembly protocol through combination of Mn^{2+} salts or $[Mn_3O(O_2CR)_6L_3]^{n+}$ triangles with flexible ligands.[19]Use of azide and carboxylate ions, showing coordinating/bridging functions, can be advantageous for fine tuning of aggregation processes and these ions are established as structural and magnetic linkers in the fields of cluster synthesis and molecular magnetism.[20] Multinuclear manganese complexes are fascinating because of their intriguing structures, involvement in sensing studies, magnetism and catalysis.[21-23] Catalytic oxidation of a variety of *o*-diphenol (or catechol) to *o*-quinone is executed by catechol oxidase in nature as found in type 3 copper proteins. Several multinuclear complexes of manganese have also been shown to promote the catalytic oxidation of catechol in laboratory condition. [24,25]

The methoxy substituted Schiff base having one alcohol-arm is known to facilitate the coordination aggregation reaction smoothly.[26] The auxiliary ligands like $MeCO_2^-$, HO^-, $O^{2-}$and N_3^- are known to be useful for extending and fine tuning the smaller aggregate to larger one through occupancy of the vacant coordination sites around the participating manganese ions.

While exploring the synthesis of new form of manganese coordination aggregate, we have reacted the –OMe substituted Schiff base 2-[(2-hydroxy-1,1-dimethyl-ethylimino)-methyl]-

phenol (H_2damp) (Chart I) toward manganese acetate premixed with sodium azide, to isolate and study the octanuclear manganese aggregate having [$Mn^{II}_2Mn^{III}_6Na^{I}_3$] core.

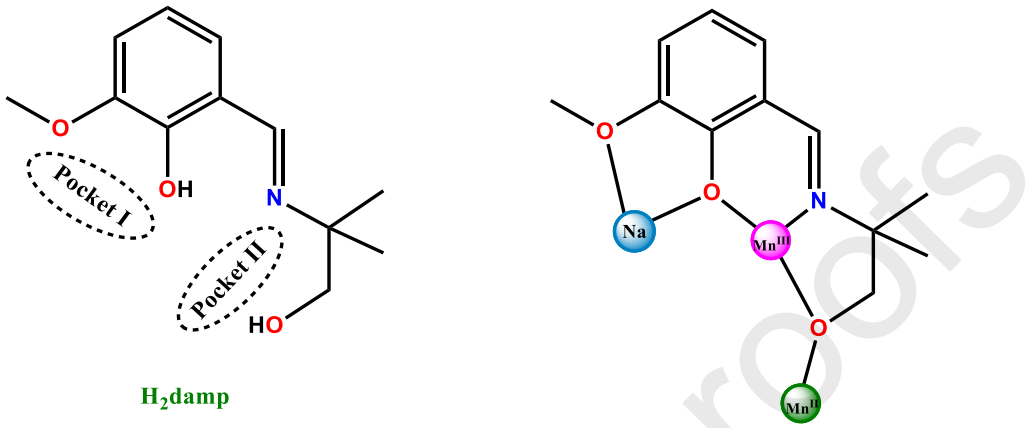

Chart I. Structure of H_2damp and its coordination modes observed in this work.

This ligand H_2damp was previously utilized to obtain [Ni_3], [Cu_4] complexes by Dey et al. [27,28] and [Mn_3], [Mn_4] complexes by Pait et al.[29] The water derived O^{2-} binds Na^+ ions from NaN_3 serve as templates to grow the final form of the compound following a new path for molecular aggregation. The structure of the complex is determined by X-ray crystallography. The solid-state magnetic properties and solution phase catalytic oxidation of catechol, mimicking the catechol oxidase function in laboratory condition have been studied.

Experimental Section

Materials and Reagents

The solvents and chemicals used in this work were obtained from commercial sources. The sources are manganese(II) acetate tetrahydrate from SRL, India, sodium azide, triethyl amine from Merck, India 2-hydroxy-3-methoxybenzaldehyde (*o*-vanillin) from Spectrochem, India and 2-amino-2-methylpropan-1-ol from Alfa Aesar, India. The chemicals used in this work were of reagent-grade and were used as received without further purification.

Caution! *Although no complications have arisen during synthesis with the reported compound, organic ligand-containing metal complexes in combination with azide ions possess potential explosiveness.*

Synthesis of Ligand

H_2damp 2-[(2-hydroxy-1,1-dimethyl-ethylimino)-methyl]-6-methoxy-phenol. The ligand H_2damp was prepared according to a previously reported procedure. H_2damp was obtained from Schiff base condensation reaction between the chosen aldehyde and its amine counterpart. To a stirred solution of 2-amino-2-methylpropan-1-ol (0.18 g, 2 mmol) in MeOH (10 mL) was added 10 mL MeOH solution of 2-hydroxy-3-methoxybenzaldehyde (0.30 g, 2 mmol) in 1:1 molar ratio. After complete addition, the solution was allowed to stir for 30 min followed by a reflux of 2 h duration. Then the whole solution was evaporated under reduced pressure to reduce the solvent volume to obtain an orange oily mass. Repeated washing was made with n-hexane to remove the unreacted reactants and finally recrystallized from methanol solution as reported previously.[30]

Synthesis of the Complex

***$[Na_3Mn^{III}_6Mn^{II}_2(damp)_6(\mu_4\text{-}O)_2(\mu_{1,3}\text{-}O_2CCH_3)_2(\mu_{1,1}\text{-}N_3)_6(\mu_{1,1,3}\text{-}N_3)(H_2O)_2]\cdot 5H_2O\cdot CH_3OH$*(1)**

Solid sodium azide (0.26 g, 4mmol) was added to a MeOH solution (10 mL) of manganese(II) acetate (0.49 g, 2mmol) resulting in a brown turbid solution. To this 10 mL MeOH solution of H_2damp (0.22 g, 1mmol) was added. The turbidity slowly dissolved yielding a clear wine red solution. After stirring this mixture for 30 min, NEt_3 (0.20 g, 2mmol) was added to it in dropwise manner. During the addition of NEt_3 the solution color changed from wine red to brown. The reaction mixture was next stirred for an additional period of 1.5 h. The whole reaction mixture was then filtered and kept for slow evaporation. After 7 days, brown crystals suitable for X-ray diffraction were obtained from the mother liquor. Yield: 0.48 g, 78%. Anal. Calc. for $C_{77}H_{106}Mn_8N_{27}Na_3O_{32}$ (2430.30 g mol^{-1}): C, 36.92; H, 4.57; N, 15.30. Found: C, 36.69; H, 4.65; N, 15.21%. Characteristic FTIR peaks (KBr, cm^{-1}; s = strong, vs = very strong, m = medium, br= broad): 3375(br), 2063(s), 1621(s), 1551(s), 1443(m). UV–vis spectra [λ_{max}, nm (ε, L mol^{-1} cm^{-1})] (MeCN solution): 222 (24900), 275 (7590), 310 (5090), 396 (1420).

Physical Measurements

The purity of the complex was examined by measuring the percentage of carbon, hydrogen, nitrogen with a PerkinElmer model 240C elemental analyzer. A Shimadzu UV–vis–NIR spectro-

photometer model UV 3100 was used for recording the solution-state electronic absorption spectra of the compounds. PerkinElmer model RX1 FTIR spectrometer was used to obtain the FTIR spectra on KBr pellets. The ESI MS analysis was performed with Bruker Esquire 3000 plus mass spectrometer. Electron paramagnetic resonance (EPR) spectra were recorded at 9.13 GHz (X-band) in continuous-wave mode with a Bruker ELEXSYS 580 X-band EPR spectrometer equipped with a standard accessory for room temperature operation (298 K). All magnetic measurements were carried out on powdered crystalline samples restrained in eicosane using a Quantum Design MPMS-XL SQUID magnetometer. Data were corrected for the diamagnetic contribution of the sample holder and eicosane by measurements, and for the diamagnetism of each compound.

Kinetic Studies. To investigate the ability of the catalytic oxidation of 3,5-di-*tert*-butyl catechol (3,5-$DTBCH_2$),1×10^{-4} M the MeOH solution of **1** was treated with 1×10^{-2} M (100 equiv.) of 3,5-$DTBCH_2$ under air saturated conditions and the reaction was monitored by UV–vis spectroscopy. The kinetics of the 3,5-$DTBCH_2$ oxidation was studied by tracking the increase of the concentration of the product 3.5-ditertiarybutylquinone (3,5-DTBQ). The concentration of the substrate 3,5-$DTBCH_2$ was always kept 100 times higher than that of the complex and the increase of the respective quinone concentration was determined at around 410 nm. Initial rate method has been followed for analyzing the kinetics for the oxidation of the substrate 3,5-$DTBCH_2$ at 25 °C. The dependence of the initial rate on the concentration of the substrate was monitored spectrophotometrically at a particular wavelength. The initial rate method showed a first-order dependence on the concentration of the complex and exhibited saturation kinetics at higher substrate concentrations. Since the complex showed saturation kinetics, a treatment based on the Michaelis-Menten model seemed to be appropriate. The kinetic parameters like binding constant (K_M), maximum velocity (V_{max}), and rate constant for the dissociation of substrates (*i.e.*, turnover number, k_{cat}) were obtained from the double-reciprocal Lineweaver–Burk plots of $1/V$ *vs.* 1/[S], using the equation $1/V = \{K_M/V_{max}\}\{1/[S]\} + 1/V_{max}$.

Method of hydrogen peroxide detection in the catalytic reaction

A modified iodometric procedure was employed to identify produced H_2O_2, if any, during the catalytic oxidation of $DTBCH_2$ using spectrophotometry.[31] Reaction mixture was prepared

using 1:100 molar mixture of complex and 3,5-DTBCH_2. To fully quench the reaction, the reaction mixture was acidified to pH 2 after one hour using H_2SO_4 (1×10^{-3} M). The product 3,5-DTBQ was extracted using CH_2Cl_2 and the aqueous layer was separated. To this aqueous layer 1 mL of 10% aqueous KI was added, which results in triiodide (I_3^-) ion formation in presence of H_2O_2, produced during catalytic cycle. Addition of few drops of ammonium molybdate (3%) solution facilitates the generation of I_3^-.[32] The triiodide ion gives a characteristic absorption band at 349 nm (ε = 26 000 L mol^{-1} cm^{-1})

Single Crystal X-ray Diffraction Analysis

Single crystal X-ray structural study of complex **1** is performed in a Bruker SMART APEX-II CCD X-ray diffractometer equipped with a graphite-monochromated Mo-Kα (λ = 0.71073 Å) radiation by the ω scan (width of 0.3° $frame^{-1}$) at 114 K with a scan rate of 5 s per frame. SAINT, SMART and XPREP software's have been used for indexing, integration and space group determination, respectively. [33] Direct method using SHELXT 2014/5 [34] is used to solve crystal structures and refined by full-matrix least squares technique using SHELXL (2014/7) programs. [35] Empirical absorption corrections (multi-scan) were carried out using SADABS program. [36] All non-hydrogen atoms were refined with anisotropic displacement parameters while hydrogen atoms were incorporated at geometrical positions and were refined using the riding model. DIAMOND software was used for presenting the molecular structures. [37] The structure showed a solvent void filled with a few electron density peaks due to disordered/diffuse solvent and cations; attempts to model this were not possible. Accordingly, the solvent mask routine in OLEX2 [38] was used to account for the contribution of the solvent. Refinement parameters for complex **1** are summarized in Table S1 and crystallographic data (excluding structure factors) have been deposited with the Cambridge Crystallographic Data Centre as supplementary publications CCDC 2344284 for complex **1**.

Results and Discussion

Synthetic Protocol. Simple single step Schiff base condensation reaction provided H_2damp. Molecular oxygen from air was utilized for partial oxidation of the metal ion centers during the reactions of the precipitates obtained from the reaction of the Mn(II) acetate and sodium azide. Controlled dissolution of these precipitates by H_2damp provided **1**. The final reaction with H_2damp typically established the efficacy of the chosen ligand system for the reactions with

initially formed $Mn(N_3)_2$ species in solution. These salts on reaction with H_2damp (1 equiv) in presence of NEt_3 resulted **1** from the reaction medium. The formation of **1** is summarized in Scheme 1, which were finally established from X-ray structure determination. (*vide supra)*

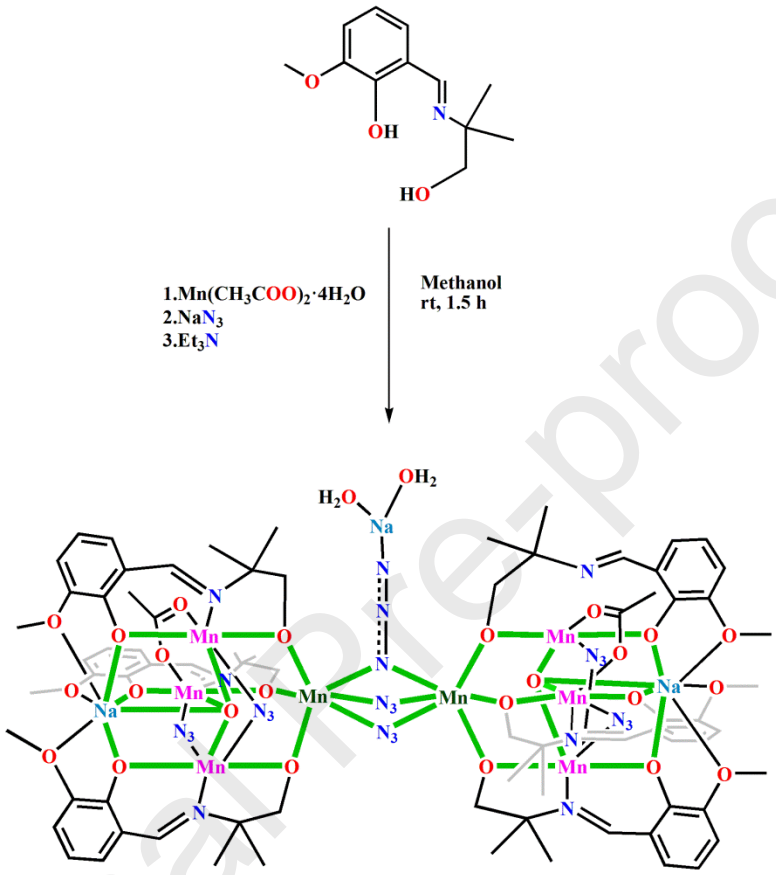

Scheme 1 Schematic for synthetic aggregation for complex **1**

Slow evaporation of the solvent from the final reaction mixture gave **1** as nice brown colored crystal in 78% yield. Several solvent molecules were needed to stabilize the crystal lattices, apart from coordinated water molecules in case of **1**. The reactions were executed in the presence of air and moisture of the laboratory environment. Interestingly in the complex structure phenolate oxygen coordination triggered oxidation of manganese ions whereas azido environment stabilized the reduced forms.

FTIR Spectral Characterization. The FTIR spectrum of the complexes was recorded on KBr pellet. The characteristic stretching vibrations of the metal ion bound –C=N function was observed at 1624 cm^{-1} for **1**. The presence of coordinated water and lattice water molecules

showed metal broad peak centered at 3375 cm^{-1} for **1.** The bridging acetates groups in **1** registered band due to $\bar{\nu}_{assym}$ and $\bar{\nu}_{sym}$ at 1551 cm^{-1} and 1443 cm^{-1} for asymmetric and symmetric stretching vibrations of the bridging carboxylate moiety.[39] The difference of these values, $\Delta\bar{\nu}$= 108 cm^{-1} is characteristic for $\mu_{1,3}$ mode of bridging. Presence of the azido coordination in **1** is confirmed from the appearance of very strong and sharp peak at 2063 cm^{-1}. (Fig. S1 in SI)

Electronic Spectral Signatures. The electronic absorption spectrum of the complex was recorded in MeCN solution. The distinctive phenoxido n→π* transition for H_2damp at 440 nm (ε, 22100 M^{-1} cm^{-1}) is blue shifted to 396 nm (ε, 14600 M^{-1} cm^{-1}) in **1** may be assigned as the ligand-to-metal ion charge-transfer (LMCT) bands. The absorption bands below 300 nm *viz.*, at 275 (ε, 25900 M^{-1} cm^{-1}) and 221 nm (ε, 74900 M^{-1} cm^{-1}) are due to the π → π* transitions of ligand origin. The d-d transition for the Mn^{III} ions ($^5E_g \rightarrow {}^5T_{2g}$ transition) in **1** was observed at around 588 nm (ε, 320 M^{-1} cm^{-1}). The high spin Mn^{II} centres in **1** did not contribute anything for *d*−*d* transitions.

Description of Crystal Structures

[$Na_3Mn^{III}_6Mn^{II}_2(damp)_6(\mu_4\text{-}O)_2(\mu_{1,3}\text{-}O_2CCH_3)_2(\mu_{1,1}\text{-}N_3)_6(\mu_{1,1,3}\text{-}N_3)(H_2O)_3]\cdot 5H_2O\cdot CH_3OH$ (1)

Complex **1** crystalizes in monoclinic $P2_{1/m}$ space group. Detail identification of the molecular constituents revealed the presence of six $damp^{2-}$ ligand anions, eight manganese ions and three sodium ions along with structure stabilizing ancillary azide and acetate ions. The molecular structure of **1** is depicted in Fig. 1 and the crystallographic data is summarized in Table S1. Important bond distances and bond angles are listed in Table S2. The functionally tetradentate ligand H_2damp, bearing three O donors and one N donor in its fully deprotonated form ($damp^{2-}$) binds one manganese ion and one sodium ion at the adjacent coordination sites utilizing the bridging capability of the central phenolate group. Three such ligand anion bound $\{NaMn^{III}(damp)\}^{2+}$ fragments are arranged around an oxido group forming two Mn_3O triangles. Each Mn_3O triangle, thus formed shows accomplishment of remaining coordination sites by two bridging azido and one bridging acetato groups.

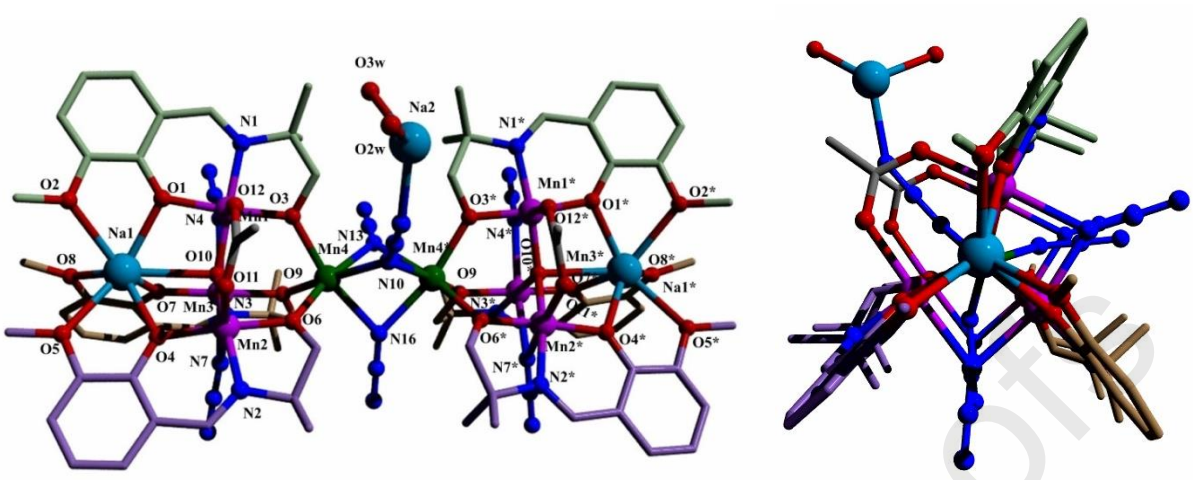

Fig. 1. Molecular structure of **1** with partial atom numbering scheme (Left). Color code: Mn^{III} magenta; Mn^{II} dark green; Na sky blue; C lavender, light green and tan; N blue; O red. View along z-axis (Right). H-atoms and lattice water molecules are omitted for clarity

Each Mn^{III} ion of Mn_3O triangle is bound to $damp^{2-}$ and simultaneously extended its coordination capacity to Na^{I} ion from one side and Mn^{II} ion from the other. The terminal alkoxido part thus took control of the fourth manganese ion in bivalent state and three such parts fulfil one face. Binding of three N_3^- ions from other face (*facial* binding) stabilized the bivalent state. These N_3^- ions showed bridging capacity to connect the other similar half. Through one of the central azido group, one $Na(H_2O)_2$ fragment is connected in *vacant tetrahedron* geometry. The Chinese lantern like core structure of **1** is depicted in Fig. 2.

The oxidation states of the manganese ions were established from the difference in bond distances and angles and further confirmed by BVS analysis.[40,41] The results for bond valance sum calculations are provided in Table S3 in SI. All the manganese ions in the multimetallic entity have distorted octahedral coordination geometry. The extent of distortions varies for the nature of the donor atoms and their positions in the ligand folds. For Mn^{III} ions two types of donor environments are observed: N_2O_4 (for Mn1, Mn2, Mn1* and Mn2*) and N_3O_3 (Mn3 and Mn3*). The Mn^{II} ions (Mn4 and Mn4*) have a N_3O_3 donor environment.

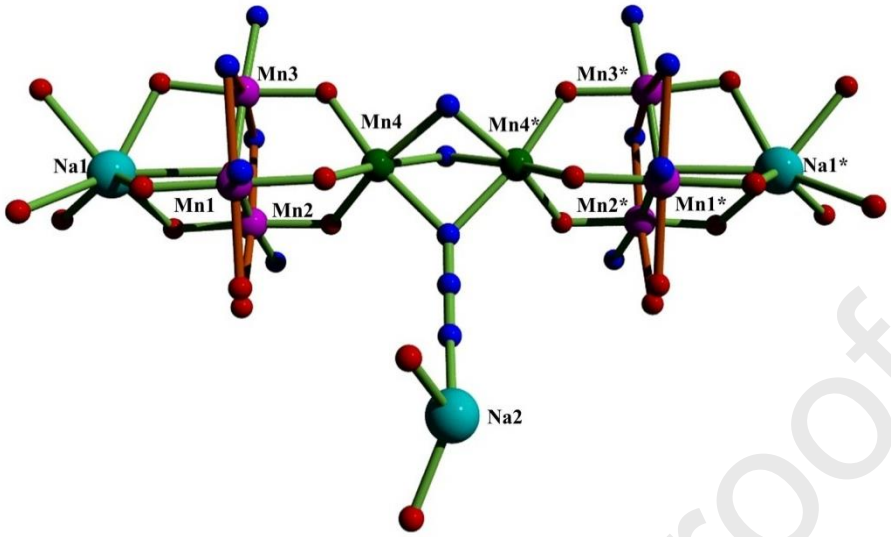

Fig. 2. Core view of complex **1** with partial atom numbering scheme. Mn^{III} JT elongation axes shown as orange bonds. Atoms with asterisks are related by the inversion center. Color code: Mn^{III} magenta; Mn^{II} dark green; Na sky blue; N blue; O red

Three $damp^{2-}$ units are required to hold the Mn_3O triangle on both sides of the molecular aggregate. Wherein the oxido bridges (O10 and O10*) connect three individual Mn^{III} centers in triangular planes and the three edges are connected by two azido and one acetato groups in an unsymmetrical fashion. The Mn^{III}–O(oxido) distances vary in 1.885−1.913 Å range. Both Na1 and Na1* are coordinated by three deprotonated phenol oxygen atoms and three methoxido oxygen atoms from three Schiff-base ligands. The two oxido donors O10 and O10* centers placed in the center of the triangle defined by the three Mn^{III} cations are shifted 0.227 Å toward the Na^{I} ions (Na1And Na1*), which are seven-coordinated, and then the O donor is a μ_4-O ligand.[42-44] The two seven-coordinated Na^{I} ions, Na1 and Na1* are below the $[Mn_3O]$ plane. *SHAPE* [45] measurements show that the coordination polyhedron around Na1 and Na1* are very close to distorted Johnson elongated triangular pyramid J7 (JETPY-7, C_{3V}) geometry and the CShM value obtained is 5.136 (Table S4 in SI) whereas the tri-coordinated Na2 ion is in distorted vacant tetrahedron geometry with CShM value of 1.264 (Table S6 in SI). The two $[Mn^{III}_3Mn^{II}Na^{I}]$ subunits are dissimilar and show different bond parameters. The $Mn^{III}\cdots Mn^{III}$ separations within these triangles having asymmetric edges, record a range from 3.137 to 3.416 Å, with longer acetato edges. The three Mn^{III} ions in each Mn_3O triangles are in distorted

octahedral geometry (Fig. 3) and the azido N and carboxylato O donors occupy the *apical* positions along the longer Jahn Teller axes. All the three Mn^{III} ions show octahedral coordination environment evident from the lowest CShMS value for six vertex polyhedra by SHAPE analysis (Table S5 in SI).

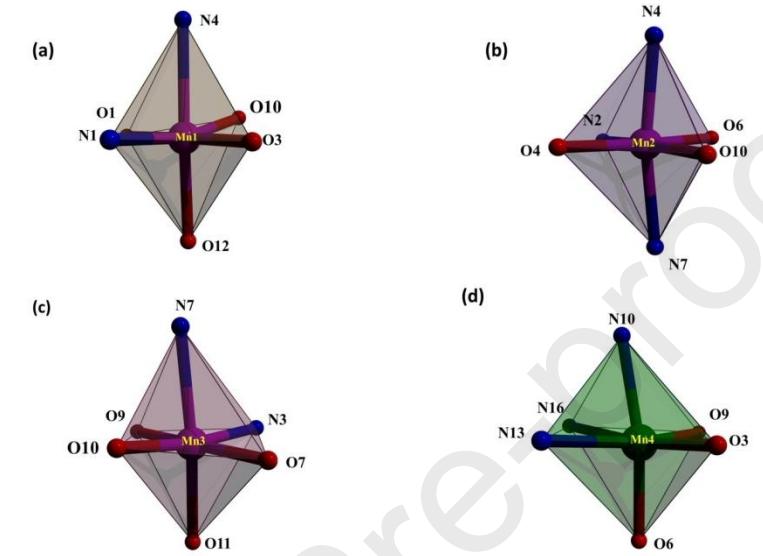

Fig. 3. Distorted octahedral geometry around the Mn^{III} and Mn^{II} ions (a-d); tetrahedral and capped prism geometry around the two types of Na^{I} ions (d-e)

The deviation from an ideal octahedral geometry for three types of manganese centers is reflected from the wide ranges of adjacent (77.04–104.45°) and opposite (162.13–177.25°) angles. The central Mn^{II} ions are also in distorted octahedral geometry, having O_3 faces from alkoxido donors of three dmp^{2-} ions and the three N_3^- groups provide the opposite N_3 face. This N_3 face connects two such Mn^{II} ions in octahedral geometry recording $Mn^{II}\cdots Mn^{II}$ separation of 3.139 Å. The three azido bridges are almost linear with N–N–N angles in the range of 178.32−179.64°.

Magnetic Properties. Direct current (dc) magnetic susceptibility measurements for **1** were performed in the range of 290-2 K under a 0.1 Tesla applied magnetic field (Fig.4). The $\chi_M T$ value of 22.5 $cm^3\ mol^{-1}$ K at 290 K is below that expected for six uncoupled Mn(III) and two uncoupled Mn(II) ions (26.8 $cm^3\ mol^{-1}$ K, for g = 2). The multiple exchange interactions present

in the $Mn^{III}_6Mn^{II}_2$ complex and the size of the spin system preclude fitting of the data to extract *J* values. Hence, the data were fitted between 290 and 50 K using the Curie-Weiss law giving a value of C = 28.3 cm^3 mol^{-1} K and θ = −50.8 cm^{-1}, consistent with predominant antiferromagnetic coupling.

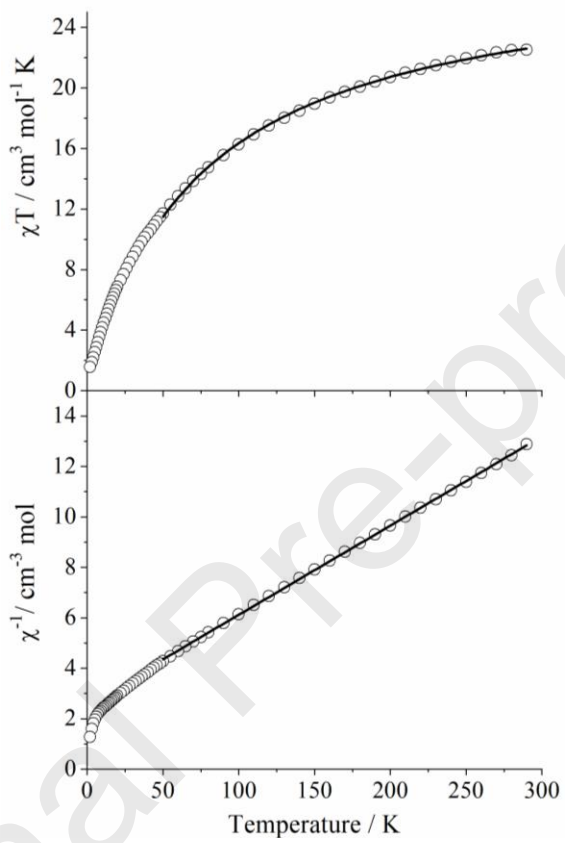

Fig.4. (top) $\chi_M T$ vs. T for **1** measured at 1 T. (bottom) χ^{-1} vs. T. The white circles are the experimental data, and the solid line corresponds to the fit of the data (see text for details)

Catalytic Catechol Oxidation using Complex 1. We were interested to examine the propensity of the ligand anion bound metal ions for oxidation reactions. Thus, we have examined the catalytic activity of **1** by evaluating its capacity for oxidation (Scheme 2) of the model substrate 3,5-di-tert-butylcatechol (3,5-DTBCH_2) to 3,5-di-*tert*-butylquinone (3,5-DTBQ) via O_2 activation to *o*-quinone in air-saturated MeOH solutions at 25 °C. [46, 47]

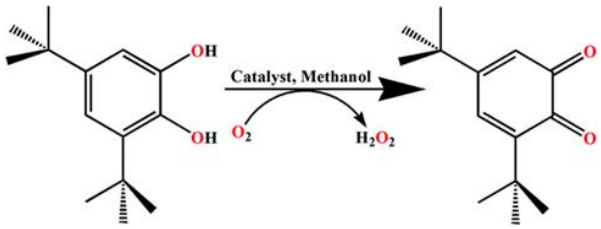

Scheme 2. Catalytic oxidation of 3,5-DTBCH$_2$ to 3,5-DTBQ in MeOH

Complex **1** showed significant catalytic oxidation of the model substrate as monitored by a standard UV–vis spectrometer. The kinetics for the oxidation of the substrate 3,5-DTBCH$_2$ has been determined by observing the increased concentration of the product, 3,5- DTBQ in solution, following the procedure reported in the Experimental Section. The solution of **1** ($\sim 1 \times 10^{-5}$ mol L^{-1}) were treated with 100 equiv. ($\sim 1 \times 10^{-3}$ mol L^{-1}) of 3,5-DTBCH$_2$under aerobic conditions and time-dependent UV-vis spectra were recorded up to 1 h. The spectral scans are given in Fig. 5 (left).

The enzyme kinetics plot for **1** is shown in Fig. 5 (right). The kinetics for the oxidation of the substrate 3,5-DTBCH$_2$ were determined by the initial rate method at 25 °C. The dependence of the initial rate on the concentration of the substrate was monitored spectrophotometrically at a particular wavelength. Moreover, the initial rate method showed a first-order dependence on the complex concentration and exhibited saturation kinetics at higher substrate concentrations.

Analysis of the experimental data shows that the Michaelis binding constant (K_M) value is $2.38 \pm 0.04 \times 10^{-4}$ whereas the V_{max} value for **1** is $(1.08 \pm 0.03) \times 10^{-6}$. Kinetic parameters for **1** are listed in Table 1.

The modified iodometric method was followed for the detection of formation of H_2O_2 in the catalytic reaction medium. The spectrophotometric method shows appearance of absorption band at ~349 nm supporting the formation of I_2 in the medium (Fig. S4), confirming the possibility of formation of H_2O_2 through the catalytic procedure.

Table 1. Kinetic parameters for the catalytic oxidation of 3,5-DTBCH$_2$ by **1** at 25 °C

Complex	Solvent	V_{max} (M s^{-1})	K_M (M)	k_{cat} (h^{-1})	k_{cat}/K_M (s^{-1} M^{-1})
1	MeOH	(1.08 ± 0.03) × 10^{-6}	(2.38 ± 0.04) × 10^{-4}	392	457

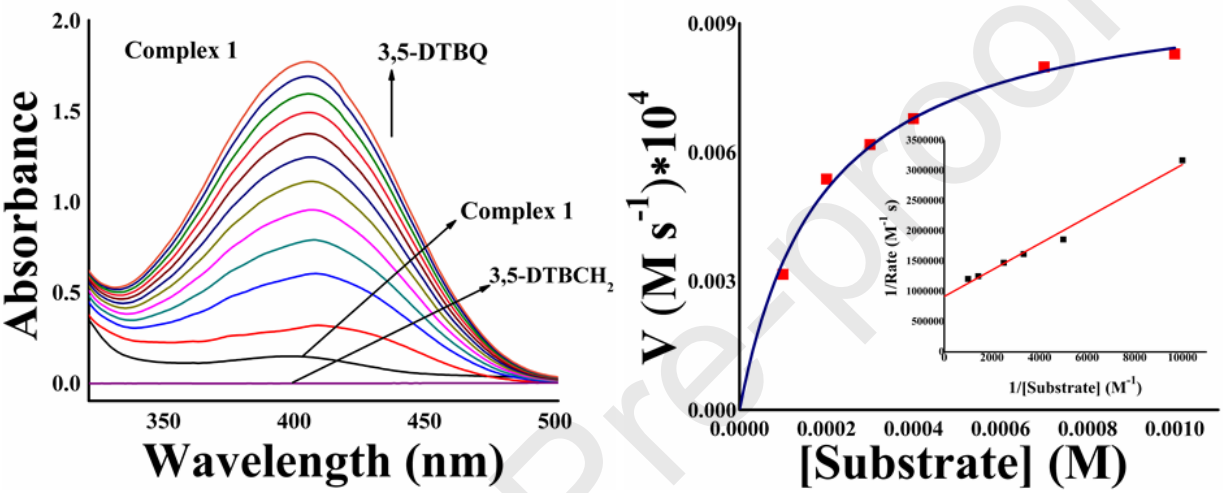

Fig. 5. UV-vis spectral changes with time for complexes **1** (conc. ~1 × 10^{-5}mol L^{-1}) upon addition of 100 fold 3,5-DTBCH$_2$(conc ~1 × 10^{-3}mol L^{-1}) in MeOH at 298 K (left). Dependence of the reaction rates on the substrate concentration for the oxidation of 3,5-DTBCH$_2$ catalyzed by complex **1** (right) in MeOH. The corresponding Lineweaver–Burk plots (inset)

The rate study was executed using the Michaelis-Menten model, and the kinetic parameters were extracted from the Lineweaver-Burk plot (insets of Fig.5 right). From the comparison of the k_{cat} (in h^{-1}) values with literature known manganese complexes (Table 2), it may be inferred that complex **1** can be accepted as a functional model of catechol oxidase.

Table 2. Selected multinuclear manganese complexes and their k_{cat} (h^{-1}) for *catechol* oxidation

Complex	**Solvent**	**k_{cat} (h^{-1})**	**Ref**
$[Mn^{III}_2Mn^{II}_4O_2(pyz)_{0.61}/(MeOH)_{0.39}(o\text{-}(NO_2)C_6H_4COO)_{10}\cdot(H_2O)\cdot\{(CH_3)_2CO\}_2]\cdot(CH_3)_2CO$	MeCN	432	48

$[Mn^{III}_2Mn^{II}_4O_2(pyz)_{0.28}/(MeCN)_{3.72}(o\text{-}(NO_2)C_6H_4COO)_{10}\cdot(H_2O)]$	MeCN	426	48
$[Mn^{III}_2Mn^{II}(O_2CMe)_4(L1)_2(H_2O)_2]\cdot 2H_2O$[a]	MeCN	8220	49
$[Mn^{III}_2Mn^{II}(O_2CCH_2Cl)_4(L1)_2(H_2O)_2]\cdot H_2O\cdot MeOH$[a]	MeCN	9011	49
$[Mn^{III}_4(\mu_3\text{-}O)(L1)_4(\mu\text{-}DMSO)(N_3)(DMSO)(H_2O)]ClO_4\cdot DMSO$[a]	MeCN	2082	49
$[Mn^{III}_4(\mu_3\text{-}O)(L1)_4(\mu\text{-}DMSO)(ClO_4)(DMSO)(H_2O)]ClO_4\cdot DMSO$[a]	MeCN	1865	49
$[Mn_4(L2)_2(\mu\text{-}O)_2(H_2O)_4](ClO_4)_4$[b]	MeCN	832	47
$[Mn_4(L3)_2(\mu_3\text{-}Cl)_2Cl_2]$ [c]	DCM/MeOH	1492.4	50
$[Mn_4(L3)_2(\mu_{1,1,1}\text{-}N_3)_2(N_3)_2]$[c]	DCM/MeOH	1431.2	50
$[Mn_3(\mu\text{-}H_2L4)_2(\mu_{1,3}\text{-}O_2CCH_3)_4(CH_3OH)_2](ClO_4)_2\cdot 4CH_3OH$[d]	MeOH	61	51
$[Mn_6(\mu_4\text{-}H_2L5)_2(\mu\text{-}H_2L6)_2(\mu_3\text{-}OH)_2(\mu_{1,3}\text{-}O_2CC_2H_5)_4](ClO_4)_2\cdot 2H_2O$[e]	MeCN	644	51
$[Mn^{III}_2Mn^{II}(L7)_2(OAc)_4(H_2O)_2]\cdot 5H_2O$[f]	MeCN	209.1347	52
$[Mn^{III}_2Mn^{II}(L8)_2(OAc)_4(CH_3OH)_2]\cdot 3CH_3OH$[g]	MeCN	197.7028	52
$[Mn_3(L9)_2\ (OAc)_4]$[h]	DMF	44.28	53
$[Na_3Mn^{III}_6Mn^{II}_2(dmp)_6(\mu_4\text{-}O)_2(\mu_{1,3}\text{-}O_2CCH_3)_2(\mu_{1,1}\text{-}N_3)_6(\mu_{1,1,3}\text{-}N_3)(H_2O)_2]\cdot 4H_2O\cdot CH_3OH$	MeOH	392	This Work

[a] H_2L1= 2-[(2-hydroxy-1,1-dimethyl-ethylimino)-methyl]-phenol

[b] HL2=1,3-bis(bis((4-methoxy-3,5-dimethylpyridin-2-yl)methyl)amino)propan-2-ol)

[c] H_2L3=*N*,*N*′-dimethyl-*N*,*N*′-bis(2-hydroxy-3-methoxy-5-methylbenzyl)ethylenediamine

[d] H_3L4= 2,6-Bis{(1-hydroxy-2-methylpropan-2-ylimino)methyl}-4-methylphenol

[e] H_5L5 = 2,6-bis[{1-hydroxy-2-(hydroxymethyl)butan-2-ylimino}methyl]-4-methylphenol; H_3L6 = 3-{(1-hydroxy-2-(hydroxymethyl)butan-2-ylimino)methyl}-2-hydroxy-5-methylbenzaldehyde)

[f]H_2L7 = 4-bromo-2-[(2-hydroxy-1,1-dimethyl-ethylimino)-methyl]-phenol

[g]H_2L8 = 2,4-dibromo-2-[(2-hydroxy-1,1-dimethyl-ethylimino)-methyl]-phenol

[h]HL9 = 4-bromo-2-(((2-morpholinoethyl)imino)methyl)phenol

Mass Spectroscopic Analysis. The solution behavior of the complex has been investigated by mass spectroscopic analysis in MeOH. The ESI-MS spectrum of the complex shows the base peak at *m/z* value of 611.1011 along with some other less intense peaks at 499.1642, 693.1024, 844.1244 and 1099.0906. (Fig. S5) Based on the calculated values of *m/z*, these peaks are assigned to the fragments $[Mn_2(damp)_2(CH_3COO)]^+$ ($C_{26}H_{33}Mn_2N_2O_8$; Calcd 611.0998), $[MnNa(damp)(N_3)(MeOH)(H_2O)_7]^+$ ($C_{13}H_{33}MnN_4NaO_{11}$; Calcd 499.1424), $[Mn_2(damp)_2(CH_3COO)(MeOH)_2(OH_2)]^+$ ($C_{28}H_{43}Mn_2N_2O_{11}$; Calcd 693.1628), $[Mn_3(damp)_3(\mu_3\text{-}O)]^+$ ($C_{36}H_{45}Mn_3N_3O_{10}$; Calcd 844.1246), and $[Mn_3Na(damp)_3(\mu_3\text{-}OH)(N_3)_3(H_2O)_4(MeOH)]H^+$ ($C_{37}H_{59}Mn_3N_{12}NaO_{15}$; Calcd 1099.2262), respectively. The catalytic proficiency of the complex on 3,5-$DTBCH_2$ was also examined by HRMS analysis. The complex was mixed with 3,5-$DTBCH_2$ in 1:100 molar ratio in MeOH and the mixture was examined by HRMS analysis after 5 min of mixing. The spectrum displays characteristic peak at 238.1839 for $[3,5\text{-}DTBSQ\cdot H_2O]^{+\cdot}$ ($C_{14}H_{22}O_3$; Calcd 238.1569). (Fig. S6) The base peak at *m/z* value of 224.1329 can be assigned to the species $[H_3damp]^+$. Other less intense peaks at *m/z* values of 469.2313 and 458.3326 can be ascribed to the catalyst-substrate associates [Mn(*o*-vanillin)(3,5-DTBSQ)(N_3)]$H^{+\cdot}$($C_{22}H_{28}MnN_3O_5$; Calcd 469.1409) and [Mn(*o*-vanillin)(3,5-DTBSQ)(MeOH)]$^{+\cdot}$($C_{23}H_{31}MnO_6$; Calcd 458.1501), respectively. In solution the hydrolysis of damp anion produced the parent *o*-vanillin molecule bound to the Mn^{III} center. Thus, the ESI-MS analysis confirms the presence of single manganese bound hydrolyzed ligand fragment, which acts as the active species during the catalytic oxidation of 3,5-$DTBCH_2$.

EPR Analysis. To gain further insight into the mechanistic pathway of the catechol oxidation reaction, solution phase EPR spectral measurements were performed. The MeOH solutions of the complex and complex-catechol mixture (1:100 molar ratio) were taken for EPR analysis. The EPR spectrum of the complex (Fig. 6) shows six hyperfine lines resulting from the Mn^{II} (^{55}Mn, I = 5/2).[54] The hyperfine lines appear at g values of 2.14, 2.08, 2.03, 1.98, 1.92 and 1.87 and A_{av} value of 93.2 G. The EPR spectrum of the mixture of complex and 3,5-$DTBCH_2$ (1:100) shows enhanced intensity of the six hyperfine lines along with appearance of a sharp radical peak at g =

2.004. This observation suggests the conversion of catalytically active ligand bound Mn^{III} species to Mn^{II} ions along with generation of an organic semiquinone radical during the oxidation procedure. From the combined ESI-MS and EPR spectral analysis a plausible mechanistic pathway is proposed in Scheme S1.

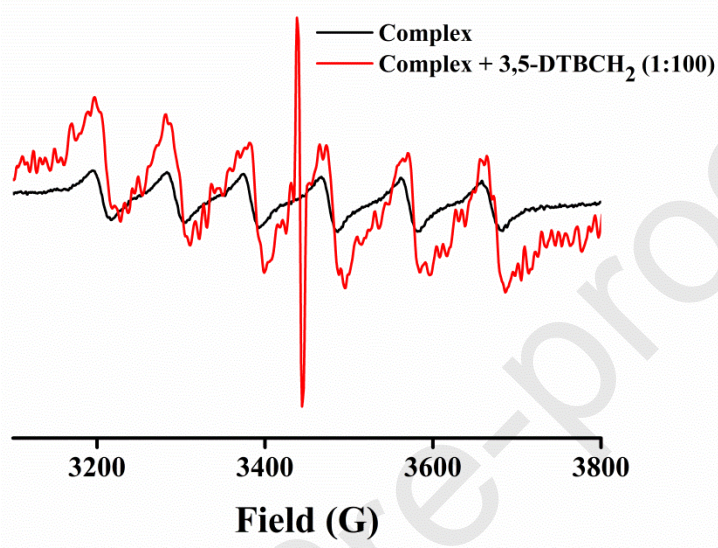

Fig. 6. EPR spectra of complex **1** (black) and 1:100 mixtures (red) of **1** with 3,5 $DTBCH_2$ in MeOH at room temperature

Conclusion

An exciting synthesis of manganese coordination cluster complex has been explored utilizing supportive secondary coordination of sodium ions. The unique and literature unknown species has been obtained from the use of stoichiometric NaN_3, rightly poised the entrapment of both the cationic and anionic parts of the salt. Three sodium ions were needed for the saturation of the available coordination pockets and stability of the sodium ion supported mixed-valence manganese complex $Mn^{II}_2Mn^{III}_6Na^{I}_3$. The complex was produced in good yield while exploring the multiple metal ion binding potency of the Schiff base H_2dmp. Interestingly the complex has a charming Chinese lantern like structural feature. The central $\{Mn^{II}_2(\mu\text{–}N_3)_3\}$ unit, in lower oxidation state joins two peripheral ligand bound $\{NaMn^{III}_3(damp)_3\}$ fragments to grow the complex **1**. The magnetic study of complex **1** indicated involvement of several exchange interactions within $Mn^{III}_6Mn^{II}_2$ network having predominant antiferromagnetic coupling. The catalytic catechol oxidation potential of the complex **1** is explored on model substrate 3,5 -

$DBTCH_2$. Solution studies established complex **1** as a catalyst for the aerobic oxidation of 3,5-$DTBCH_2$ to 3,5-DTBQ with a turnover number of 392 h^{-1}. The study confirmed the involvement of ligand anion bound manganese(III) center during catalysis through generation of catechol based organic radical. Combined use of the EPR and mass spectrometry studies identified the catalytic reaction pathway.

Declaration of Competing Interest

The authors declare that they have no known competing financial interests or personal relationships that could have appeared to influence the work reported in this paper.

Acknowledgements

KC is thankful to the CSIR and DST, India for the financial support. We are also thankful to DST, New Delhi, for providing the Single Crystal X-ray Diffractometer facility to the Department of Chemistry, IIT Kharagpur under its FIST program. M. M. thanks the University of Glasgow for financial support.

References

1. R. Ogawa, T. Suzuki, M. Hirotsu, N. Nishi, Y. Shimizu, Y. Sunatsuki, Y. Teki, I. Kinoshitad, Dalton Trans. 48 (2019) 13622–13629.
2. R. Bikas, P. Mirzakhani, N. Noshiranzadeh, J. Sanchiz, M. S. Krawczyk, D. A. Kalofolias, T. Lis, Inorg. Chim. Acta 505 (2020) 119461.
3. R. Herchel, R. Boc̆, M. Gembický, K. Falk, H. Fuess, W. Haase, I. Svoboda, Inorg. Chem. 46 (2007) 1544–1546.
4. B. M. Hoffman, D. R. Dean, L. C. Seefeldt, Acc. Chem. Res. 42 (2009) 609−619.
5. K. N. Ferreira, T. M. Iverson, K. Maghlaoui, J. Barber, S. Iwata, Science. 303 (2004) 1831−1838.
6. A. Zouni, H. T. Witt, J. Kern, P. Fromme, N. Krauss, W. Saenger, P. Orth, Nature. 2001 (409) 739–743.
7. J. Biesiadka, B. Loll, J. Kern, K. D. Irrgang, A. Zouni, Phys. Chem. Chem. Phys. 6 (2004) 4733−4736.
8. N. Kamiya, J. R. Shen, Proc. Natl. Acad. Sci. U. S. A. 100 (2003) 98−103.
9. A. Z. Lekuona, J. M. Seco, E. Colacio, Coord. Chem. Rev. 441 (2021).
10. R. D. Cannon, R. P. White, Prog. Inorg. Chem. 36 (1988) 195–298.
11. S. M. J. D. Aubin, M. W. Wemple, M. B. Maple, G. Christou, D. N. Hendrickson, J. Am. Chem. Soc. 120 (1998) 839–840.

12. J. Yoo, E.K. Brechin, A. Yamaguchi, M. Nakano, J. C. Huffman, A. L. Maniero, L. C. Brunel, K. Awaga, H. Ishimoto, G. Christou, D. N. Hendrickson, Inorg. Chem. 39 (2000) 3615–3623.
13. A. T. Tasiopoulos, A. Vinslava, W. Wernsdorfer, K. A. Abboud, G. Christou, Angew. Chem. 116 (2004) 2169–2173.
14. S. Koizumi, M. Nihei, M. Nakano, H. Oshio, Inorg. Chem. 44 (2005) 1208–1210.
15. N. E. Chakov, A. E. Thuijs, W. Wernsdorfer, A. L. Rheingold, K.A. Abboud, G. Christou, Inorg. Chem. 55 (17) (2016) 8468-8477.
16. G. Rajaraman, M. Murugesu, E. C. Sanudo, M. Soler, W. Wernsdorfer, M. Helliwell, C. Muryn, J. Raftery, S. J. Teat, G. Christou, E. K. Brechin, J. Am. Chem. Soc. 126 (2004) 15445–15457.
17. A. Ferguson, K. Thomson, A. Parkin, P. C. Constantinos, J. Milios, E. K. Brechin, M. Murrie, Dalton Trans. (2007) 728–730.
18. M. Manoli, R. D. L. Johnstone, S. Parsons, M. Murrie, M. Affronte, M. Evangelisti, E. K. Brechin, Angew. Chem. Int. Ed. 46 (2007) 4456–4460.
19. J. Cano, T. Cauchy, E. Ruiz, C. J. Milios, C. C. Stoumpos, T. C. Stamatatos, S. P. Perlepes, G. Christou, E. K. Brechin, Dalton Trans. (2008) 234–240.
20. Q. Yue, E. Q. Gao, Coord. Chem. Rev. 382 (2019) 1–31.
21. Z. Lu, M. Yuan, F. Pan, S. Gao, D. Zhang, D. Zhu, Inorg. Chem. 45 (2006) 3538–3548.
22. Y. Sawada, W. Kosaka, Y. Hayashi, H. Miyasaka, Inorg. Chem. 51 (2012) 4824–4832.
23. H. Miyasaka, R. Clerac, W. Wernsdorfer, L. Lecren, C. Bonhomme, K. Sugiura, M. Yamash ita, Angew. Chem. Int. Ed. 43 (2004) 2801–2805.
24. A. Hazari, L. K. Das, R. M. Kadam, A. Bauzá, A. Frontera, A. Ghosh, Dalton Trans. 44 (2015) 3862–3876.
25. S. Maity, P. Mahapatra, T. K. Ghosh, R. M. Gomila, A. Frontera, A. Ghosh, Dalton Trans. 50 (2021) 4686–4699
26. S. Manna, E. Zangrando, H. Puschmann, S.C. Manna, Polyhedron. 162 (2019), 285-292.
27. M. Dey, C. P. Rao, P. K. Saarenketo, K. Rissanen, Inorg. Chem. Commun. 5 (2002) 380–383.
28. M. Dey, C. P. Rao, P. K. Saarenketo, K. Rissanen, Inorg. Chem. Commun. 5 (2002) 924–928.
29. M. Pait, M. Shatruk, D. Ray, Dalton Trans. 44 (2015) 11741–11754.
30. A. Bhanja, S. R. Chaudhuri, A. B. Canaj, S. P. Vyas, F. Ortu, L. Smythe, M. Murrie, R. Goswami, D. Ray, Dalton Trans. 52 (2023) 3795–380.
31. S. Z. Senior, L. L. Mans, H. D. V. Guilder, K. A. Kelly, M. P. Hendrich, T. E. Elgren, Biochemistry 42(2003) 4392–4397.
32. A. Neves, L. M. Rossi, A. J. Bortoluzzi, B. Szpoganicz, C. Wiezbicki, E. Schwingel, W. Haase, S. Ostrovsky, Inorg. Chem. 41(2002) 1788–1794.
33. SAINT, SMART and XPREP, Siemens Analytical X-ray Instruments Inc., Madison, WI, (1995).
34. G. M. Sheldrick SHELXT - Integrated space-group and crystal-structure determination Acta Cryst. A. 71 (2015) 3–8.
35. G. M. Sheldrick, Crystal structure refinement with SHELXL, Act Cryst. C 71 (2015) 3–8.
36. G. M. Sheldrick SADABS Software for Empirical Absorption Correction; Institute fur An organische Chemieder Universitat (1996).

37. DIAMOND, Visual Crystal Structure Information System, version 3.1; Crystal Impact: Bonn, Germany, (2004).
38. O.V. Dolomanov, L. J. Bourhis, R. J. Gildea, J. A. K. Howard, H. Puschmann, J. Appl. Cryst. 42 (2009) 339–341.
39. K. Chattopadhyay, B. K, Shaw, S. K. Saha, D. Ray, Dalton Trans. 45 (2016) 6928–6938.
40. I. D. Brown, D. Altermatt, Acta Crystallogr. Sect. B: Struct. Sci. 41 (1985) 244−247.
41. I. D. Brown, Chem. Rev. 109 (2009) 6858−6919.
42. L. Cong, X. Qin, W. Sun, Y. Wang, S. Ding, Z. Liu, New J. Chem. 38 (2014) 545–551.
43. J. Mayans, M. Font-Bardia, L. Di Bari, A. Escuer, Chem. Eur. J. 24 (2018) 18705–18717.
44. J. Mayans, M. Font-Bardia, A. Escuer, Inorg. Chem. 57 (2018) 926–929.
45. SHAPE, version 2.0, Electronic Structure Group, Universiat de Barcelona, Barcelona, Spain, (2010).
46. P. Chakraborty, I. Majumder, K. S. Banu, B. Ghosh, H. Kara, E. Zangrando, D. Das, Dalton Trans. 45 (2016) 742–752.
47. R. Kumar, R. Keshri, K. Prodhan, K. Shaikha, A. Draksharapu, Dalton Trans. 52 (2023) 15412 –15419.
48. P. Kar, Y. Ida, T. Kanetomo, M.G. Drew, T. Ishida, A. Ghosh, Dalton Trans. 44(2015), 9795-9804.
49. M. Pait, M. Shatruk, D. Ray, Dalton Trans. 44 (2015) 11741–11754.
50. A. Das, M. Chakraborty, S. Maity, A. Ghosh, Dalton Trans. 48 (2019) 9342 –9356.
51. K. Chattopadhyay, G. A. Craig, M. J. H. Ojea, M. Pait, A. Kundu, J. Lee, M. Murrie, A. Frontera, D. Ray, Inorg. Chem. 56 (2017) 2639–2652.
52. S. Dasgupta, S. Karim, S. Khatua, A. Adhikary, K. Acharya, E. Zangrando, S. Maity, D. Das, New J. Chem. 47 (2023) 9681–9691.
53. A. Sarkar, A. Chakraborty, A. Adhikary, S. Maity, A. Mandal, D. Samanta, P. Ghosh, D. Das, Dalton Trans. 48 (2019) 14164–14177.
54. E. Garribba, G. Micera, Magn. Reson. Chem. 44 (2006) 11–19.

Graphical Abstract

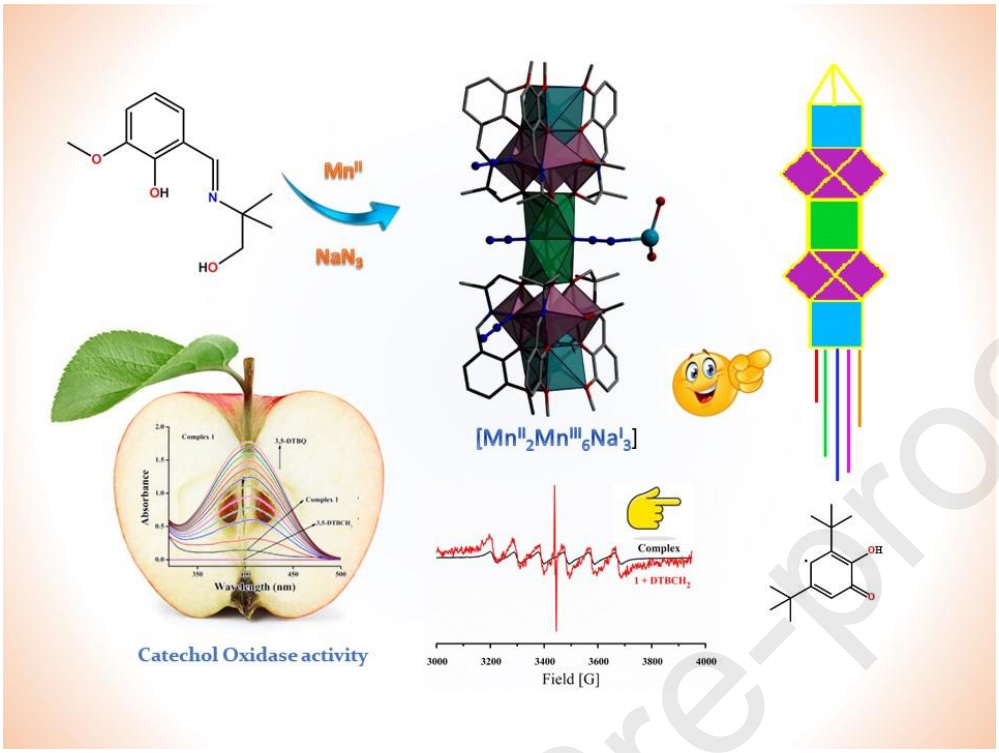

Graphical Abstract

Synopsis

Ligand H_2damp with potential donor atom bearing flexible side arms lead to $[Mn^{II}_2Mn^{III}_6Na^{I}_3]$ coordination aggregates of fascinating molecular structure which show overall antiferromagnetic interactions between the manganese ions. The complex has been explored as model for catecholase activity.

Highlights

1. A new mixed-valence [$Mn^{II}_2Mn^{III}_6Na^{I}_3$] coordination aggregate has been synthesized.
2. The complex possesses unique Chinese Lantern Shaped topology.
3. The variable temperature magnetic behaviour revealed antiferromagnetic interactions prevailed between Mn centers.
4. Catecholase activity of the synthesized complex was explored.